Journal of Extracellular Biology

TECHNICAL REPORT OPEN ACCESS

A One-Step Workflow for Size-Based Separation of Extracellular Vesicles With Integrated Surface Marker Detection

Lien Lippens[1,2,3] | Niké Guilbert[1,2] | Sofie Van Dorpe[1,2,3] | Sarah Deville[1,2,4] | Robin Boiy[1,2] | Quentin Roux[1,2,5] | Nicolaas Lumen[2,6] | Ilkka Miinalainen[7] | Pekka Rappu[8] | Katrien Vandecasteele[2,9] | Hannelore Denys[2,3] | Bruno De Geest[2,10] | Olivier De Wever[1,2] | An Hendrix[1,2]

[1]Laboratory of Experimental Cancer Research, Department of Human Structure and Repair, Ghent University, Ghent, Belgium | [2]Cancer Research Institute Ghent (CRIG), Ghent, Belgium | [3]Medical Oncology, Department of Internal Medicine and Pediatrics, Ghent University Hospital, Ghent, Belgium | [4]Laboratory for Molecular Diagnostics, Department of Clinical Biology, Jessa Hospital, Hasselt, Belgium | [5]CRCI[2]NA, Nantes Université, INSERM, CNRS, Nantes, France | [6]Department of Urology, Ghent University Hospital, Ghent, Belgium | [7]Biocenter Oulu, University of Oulu, Oulu, Finland | [8]Department of Life Technologies and InFLAMES Flagship, University of Turku, Turku, Finland | [9]Radiotherapy, Department of Human Structure and Repair, Ghent University, Ghent, Belgium | [10]Department of Pharmaceutics, Ghent University, Ghent, Belgium

Correspondence: An Hendrix (An.Hendrix@UGent.be)

Received: 27 August 2025 | **Revised:** 28 November 2025 | **Accepted:** 22 December 2025

Keywords: AF4 | biomarker | cancer | extracellular vesicles | field-flow fractionation | liquid biopsy

ABSTRACT

Extracellular vesicles (EVs) are released by diverse cell types in biofluids and are increasingly studied in liquid biopsies as diagnostic and prognostic biomarkers for various diseases, including cancer. Typically, the analysis of EV-associated biomarker characteristics such as size and surface markers requires pre-purification from large volumes of complex biofluids, leading to longer turnaround times and more technical variability. To overcome these limitations, we developed a one-step workflow that combines size-based separation with size and surface marker characterisation of EVs in minute volumes from different biological fluids. We coupled a multi-angle light scattering detector (MALS) and a fluorescent light detector (FLD) in-line with the asymmetrical flow field-flow fractionation (AF4) equipment. The AF4-MALS-FLD workflow was optimised to enable the analysis of EV surface markers CD9, CD63 and CD81, and cancer biomarkers PSMA, EpCAM and HER2 in samples of increasing complexity, including purified EV preparations, cell culture supernatant, urine and blood plasma. Proof-of-concept was gained for the detection of PSMA-positive EVs in urine from prostate cancer patients and discrimination of breast cancer patients from healthy donors by quantifying EpCAM- or HER2-positive EVs in blood plasma. In conclusion, using low-volume biofluids, the one-step AF4-MALS-FLD workflow holds potential for fast and robust EV biomarker detection.

Abbreviations: AF4, asymmetrical flow field-flow fractionation; BSA, bovine serum albumin; dSTORM, direct stochastic optical reconstruction microscopy; EpCAM, epithelial cell adhesion molecule; EVDS, extracellular vesicle-depleted serum; EVs, extracellular vesicles; FBS, fetal bovine serum; FLD, fluorescent light detection; HER2, human epidermal growth factor receptor 2; LC-MS/MS, liquid chromatography-tandem mass spectrometry; LFQ, label-free quantification; LOD, limit of detection; MALS, multi-angle light scattering; NTA, nanoparticle tracking analysis; ODG, OptiPrep^{TM} density gradient; PBS, phosphate buffered saline; PE, phycoerythrin; PES, polyethersulfone; PSMA, prostate-specific membrane antigen; RC, regenerated cellulose; R_{rms}, root mean square radius; SDS, sodium dodecyl sulphate; SMLM, single-molecule localisation microscopy; TEM, transmission electron microscopy; THP, Tamm-Horsfall protein; UV, ultraviolet.

Lien Lippens and Niké Guilbert contributed equally to this work.

1 | Introduction

Extracellular vesicles (EVs) are nanosized particles with a size between 30 and 1000 nm, mediating communication between cells (Hendrix et al. 2023). They consist of a lipid bilayer containing surface proteins that protect them from clearance from the circulation, guide them to specific organs and regulate capture by recipient cells (Hoshino et al. 2015; Kamerkar et al. 2017; Costa-Silva et al. 2015; Tkach and Théry 2016). EVs are present in multiple biofluids such as urine and blood, and since the surface proteins of EVs reflect the cell of origin, EV surface markers show potential as diagnostic and prognostic biomarkers in various diseases, including cancer (Fais et al. 2016; Kalluri 2016). Examples of EV surface markers include prostate-specific membrane antigen (PSMA) in urine from prostate cancer patients (Dhondt et al. 2020) and epithelial cell adhesion molecule (EpCAM) or human epidermal growth factor receptor 2 (HER2) in blood plasma from breast cancer patients (Menck et al. 2017; Kabe et al. 2018). However, current methods to analyse EV-associated biomarker characteristics such as size and surface marker proteins often necessitate multi-step (pre-)processing of the biofluid matrix. This induces technical variability, long turnaround time and/or low EV yields, hampering the clinical translation of EV biomarkers (Vergauwen et al. 2021; Van Dorpe et al. 2024).

The presence of non-EV particles and soluble ectodomains of transmembrane protein surface markers poorly separated from EVs negatively impacts downstream analysis (Hendrix 2021; De Wever and Hendrix 2019). To tackle these issues, we present a workflow that combines size and surface marker characterisation with in situ separation of the EVs from their matrix. This workflow includes size separation by asymmetrical flow field-flow fractionation (AF4) coupled to size characterisation by multi-angle light scattering (MALS) and surface marker identification by fluorescent light detection (FLD). We previously optimised this workflow using fluorescent recombinant EVs (Geeurickx et al. 2021). AF4 separates particles by size using two perpendicular flows (Giddings et al. 1976; Wahlund and Giddings 1987) and separates EVs from non-EV particles like exomeres in EV preparations from cell cultures, and proteins as well as lipoprotein particles in blood plasma (Zhang et al. 2018; Kim et al. 2020; Wu et al. 2020; Ashby et al. 2014; Kim et al. 2022). However, EV surface marker characterisation based on AF4-MALS-FLD has not yet been explored.

Here, we present a one-step workflow combining real-time separation of EVs from complex biofluids with size characterisation and surface protein detection. The workflow was first optimised using pre-purified EVs from cell culture supernatant, demonstrating the capacity to identify multiple EV surface markers (CD9, CD63 and CD81) and surface markers with biomarker potential in prostate and breast cancer (PSMA, EpCAM and HER2). Subsequently, specificity and robustness were tested in complex matrices such as cell culture supernatant, urine and blood plasma. The presented workflow detects PSMA-positive EVs in urine of prostate cancer patients and discriminates breast cancer patients from healthy volunteers by EpCAM or HER2 labelling in blood plasma. In conclusion, we developed an AF4-MALS-FLD labelling workflow to simultaneously separate and detect EV surface markers, validated its use in complex matrices and showed its potential to discriminate cancer patients from healthy controls.

2 | Materials and Methods

2.1 | Cell Culture

Three human breast cancer cell lines: MCF-7 (cat no. HTB-22), MDA-MB-231 (cat no. HTB-26) and SK-BR-3 (cat no. HTB-30) were purchased from the American Type Culture Collection and were cultured using Dulbecco's minimal essential medium (DMEM) (cat no. 41965039, Thermo Fisher Scientific). The human prostate cancer cell line: LNCaP (cat no. CRL-1740) was cultured using the Roswell Park Memorial Institute (RPMI) 1640 medium (cat no. 21875034, Thermo Fisher Scientific). The medium was supplemented with 10% heat-inactivated foetal bovine serum (FBS) (cat no. ATCC-30-2030, LGC Standards), 100 U/mL penicillin and 100 µg/mL streptomycin (cat no. 15070063, Thermo Fisher Scientific). Cells were expanded and maintained as a monolayer at 37°C in a humidified atmosphere of 5% CO_2 in air and were passaged at 70%–80% confluency in T175 flasks (cat no. 734-2315, VWR). Cell cultures were regularly tested and confirmed negative for mycoplasma contamination using the MycoAlert Mycoplasma Detection Kit (cat no. LT07-318, Lonza).

2.2 | EV Preparation

For the separation of EVs from conditioned cell culture supernatant, cells were seeded in 5-layer falcon cell culture multi-flasks (875 cm^2) (cat no. 353144, Corning). When a confluency of 70%–80% was reached, the cells were washed three times with DMEM supplemented with 0.5% EV-depleted serum (EVDS) and incubated for 24 h with DMEM supplemented with 0.5% EVDS. EVDS was obtained by centrifugation of FBS for 18 h at 100,000 g and subsequently filtered through a 0.2 µm cellulose acetate filter (cat no. A21320, Cytiva). Conditioned cell culture supernatant was harvested from 4 multi-layer falcon cell culture multi-flasks (a total of 3500 cm^2) and centrifuged for 10 min at 200 g and 4°C, followed by a 0.45 µm cellulose acetate filtration step (cat no. 734-5064, VWR). Conditioned cell culture supernatant was subsequently concentrated approximately 300 times to a final volume of 1 mL using Centricon Plus-70 centrifugal filters with a 10 kDa nominal molecular weight limit (cat no. UFC701008, Merck Life Science). Following collection of the supernatant, cell numbers and viability were measured on a Countess Automatic Cell Counter (Thermo Fisher Scientific) using a 0.1% trypan blue exclusion test included in the kit. Approximately 4.12×10^8 LNCaP cells, 6.62×10^8 MCF-7 cells, 3.26×10^8 MDA-MB-231 cells and 4.37×10^8 SK-BR-3 cells are counted for four multi-flasks. Cell viability between 90% and 97% was measured.

To prepare the OptiPrep™ density gradient (ODG), a working solution was prepared by combining the OptiPrep™ stock solution (60% (w/v) aqueous iodixanol solution) (cat no. AXI-1114542, Axis-Shield) with the working buffer (0.25 M sucrose, 6 mM ethylenediaminetetraacetic acid (EDTA), 60-mM Tris-HCl (pH 7.4)) (Van Deun et al. 2014). Subsequently, solutions of 5%, 10%, 20% and 40% OptiPrep™ were prepared by mixing appropriate amounts of the OptiPrep™ working solution and

homogenisation buffer (0.25 M sucrose, 1 mM EDTA, 10 mM Tris-HCl (pH 7.4)). A discontinuous top-down ODG was prepared by layering 4 mL 40%, 4 mL 20%, 4 mL 10%, and 3.5 mL 5% OptiPrep™ fractions on top of each other in a 16.8 mL open top polyallomer tube (cat no. 337986, Beckman Coulter). The concentrated cell culture supernatant (1 mL) was loaded on top of this gradient. The preparation of the gradient was performed by a Biomek 4000 pipetting robot using a custom-made script (Beckman Coulter) (Van Dorpe et al. 2023). The gradient was centrifuged for 18 h at 100,000 g at 4°C (acceleration: max, deceleration: 9) in an SW 32.1 Ti rotor (r_{avg} = 11.36 cm adjusted *k*-factor = 298.0) (Beckman Coulter). After centrifugation, 1 mL fractions were collected from the top of the gradient, and the EV-rich fractions (fractions 9 and 10: density 1.096–1.113 g/mL) were pooled, diluted to 16 mL in the phosphate buffered saline (PBS) (pH 7.2) (cat no. 20012019, Thermo Fisher Scientific), and centrifuged for 3 h at 100,000 g and 4°C (SW 32.1 Ti rotor) (Beckman Coulter). The resulting pellet was resuspended in 100 µL PBS and stored at −80°C.

2.3 | Protein Analysis

Protein concentrations of cell lysates, obtained in Laemmli lysis buffer (0.125 M Tris-HCl [pH 6.8], 10% glycerol, 2.3% sodium dodecyl sulphate (SDS)), were determined using the Bio-Rad DC Protein Assay (cat no. 500-0113/500-0114/500-0115, Bio-Rad). Protein concentrations of EVs were measured using the fluorometric Qubit Protein Assay (cat no. Q33211, Thermo Fisher Scientific) and the Qubit Fluorometer 3.0 (Thermo Fisher Scientific) according to the manufacturer's instructions. Samples were lysed with SDS (cat no. L3771, Merck Life Science) by diluting the sample 1:1 in 0.4% SDS prior to protein concentration measurement.

2.4 | Western Blot Analysis

Cell lysates were dissolved in reducing sample buffer 1.5x (0.125 M Tris-HCl [pH 6.8], 15% glycerol, 3.45% SDS, 5% 2-mercaptoethanol, 1.25% bromophenol blue), while EV samples were dissolved in reducing sample buffer 4.0x (0.5 M Tris-HCl [pH 6.8], 40% glycerol, 9.2% SDS, 5% 2-mercaptoethanol, 1.25% bromophenol blue). Samples were subsequently boiled at 95°C for 5 min. Unless otherwise specified, equal amounts of proteins were used for protein analysis. Proteins were separated by SDS-polyacrylamide gel electrophoresis (SDS-PAGE) and transferred to nitrocellulose membranes (cat no. 162-0115, Bio-Rad). Membranes were blocked for 30 min in blocking buffer (5% non-fat milk in PBS with 0.5% Tween-20 (cat no. P1379, Merck Life Science) or 5% bovine serum albumin (BSA) (cat no. 10735108001, Roche) in PBS with 0.5% Tween-20 for CD9) and incubated with primary antibodies overnight at 4°C. After extensive washing with blocking buffer, secondary antibodies were added for 45 min at room temperature. After final washing, the chemiluminescence substrate (Western-Bright Sirius) (cat no. K-12043-D10, Advansta) was added, and imaging was performed using a Proxima 2850 Imager (IsoGen Life Sciences).

The following primary and secondary antibodies were used for western blot analysis: mouse monoclonal anti-Alix (1:1000) (cat no. 2171S, Cell Signaling Technology), rabbit monoclonal anti-CD9 (1:1000) (cat no. 13403S, Cell Signaling Technology), rabbit monoclonal anti-Syntenin-1 (1:1000) (cat no. ab133267, Abcam), mouse monoclonal anti-TSG101 (1:1000) (cat no. sc-7964, Santa Cruz Biotechnology), rabbit monoclonal anti-PSMA (1:1000) (cat no. 12702S), mouse monoclonal anti-EpCAM (1:1000) (cat no. 2929S, Cell Signaling Technology), rabbit monoclonal anti-HER2 (1:1000) (cat no. 2165S, Cell Signaling Technology), mouse monoclonal anti-GAPDH (1:2500) (cat no. G8795, Merck Life Science), sheep anti-mouse horseradish peroxidase-linked (1:3000) (cat no. NA931V, GE Healthcare Life Sciences) and donkey anti-rabbit horseradish peroxidase-linked antibody (1:8000) (cat no. NA934V, GE Healthcare Life Sciences).

2.5 | Nanoparticle Tracking Analysis (NTA)

NTA was performed using a NanoSight LM10-HS microscope (Malvern Panalytical) equipped with a 488 nm laser and an automatic syringe pump system. Three videos of 30 s were recorded for each sample with a camera level of 13, a detection threshold of 3, and a syringe pump infusion speed of 20. Temperature was measured throughout the measurements. The videos were analysed with NTA software 3.4 with auto settings for blur, minimum track length and maximum jump distance. Samples were diluted in PBS (pH 7.2) to obtain a particle concentration within the optimal concentration range of the NTA software ($3 \times 10^8 - 1 \times 10^9$ particles/mL).

2.6 | Transmission Electron Microscopy (TEM)

EV samples were incubated on formvar-coated glow-discharged copper grids for 20 min. Grids were washed two times with PBS and subsequently fixed by incubating the grid with glutaraldehyde in PBS for 5 min. Grids were washed with water and subsequently stained with neutral uranyl acetate for 5 min and coated with methylcellulose/uranyl acetate for 10 min. Grids were air-dried at room temperature and analysed in a Tecnai Spirit transmission electron microscope (FEI Company). Images were captured by a Quemesa charge-coupled device camera (Olympus Corporation). Images were quantified by ImageJ version 1.8.0. EVs were tracked manually, and for each EV the diameter was assessed. The size distribution was obtained for three images per sample.

2.7 | Single-Molecule Localisation Microscopy (SMLM)

EV samples separated from cell culture supernatant were incubated with antibodies and subsequently immobilised on microfluidic glass slides using the ONI EV profiler kit version 2 (Oxford NanoImager (ONI)) to the manufacturer's instructions and stained using the pan-EV (Alexa Fluor 488) stain. The ONI nanoimager (oil-immersion objective 100x, NA 1.4, Olympus) was calibrated for direct stochastic optical reconstruction microscopy (dSTORM) analysis using 100 nm TetraSpeck microspheres (cat no. T7279, Thermo Fisher Scientific) diluted in PBS (pH 7.2) and immobilised on a glass substrate. Images were acquired via dSTORM using 50%, 50% and 40% power on the 488, 561 and 640 nm laser, respectively. Per channel 1000 images were recorded for localisation mapping. Images were analysed using the CODI

platform (alto.codi.bio). A drift correction was applied, and a lower threshold of 200 photons was used. Three fields of view were acquired. Quantification of colocalisations was performed with a limit of 200 nm in radius.

The following antibodies were used for ONI experiments: breast cancer-derived EV samples were incubated with Alexa Fluor 555 conjugated monoclonal anti-EpCAM (1 μg/mL) (cat no. 5488S, Cell Signaling Technology) and Alexa Fluor 647 conjugated monoclonal anti-HER2 (8.5 μg/mL) (cat no. NBP2-34643AF647, Novus Biologicals).

2.8 | Urine Samples

Urine samples were collected from one healthy volunteer and five prostate cancer patients in a sterile recipient according to the approval of the ethical committee (EC/2019/1506) of Ghent University and in accordance with relevant guidelines. The characteristics of participants are described in Table S1. Urine samples were centrifuged for 10 min at 1000 g and 4°C using an Eppendorf 5810R (Eppendorf) benchtop centrifuge with an A-4-62 swinging bucket rotor. Cell-free urine supernatant was collected (leaving approximately 0.5 cm urine above the cell pellet), transferred to cryovials and stored at −80°C. Upon thawing, urine samples were concentrated 10 times using Amicon Ultra-2 centrifugal filters with a 10 kDa nominal molecular weight limit (cat no. UFC201024, Merck Life Science).

2.9 | Blood Plasma Samples

Collection of blood plasma samples was performed according to the approval of the ethical committee (EC/2014/0655) of Ghent University and in accordance with relevant guidelines. The characteristics of participants are described in Tables S2 and S3. Venous blood was collected from healthy female volunteers and early-stage breast cancer patients prior to any type of therapy. Blood was collected in 9 mL Vacuette NC Coagulation sodium citrate 3.2% tubes (cat no. 455322, Greiner Bio-One) (Dhondt et al. 2023) and processed within 2 h after blood collection. Blood was centrifuged two times at 2500 g for 15 min at room temperature using an Eppendorf 5810R (Eppendorf) benchtop centrifuge with an A-4-62 swinging bucket rotor. Platelet-depleted plasma was transferred to cryovials and stored at −80°C.

2.10 | EV Labelling

EV samples separated from cell culture supernatant (4×10^{10} particles as measured by NTA, unless differently specified) were incubated with 14 μL of BSA (0.2% w/v) in PBS (pH 7.2) and phycoerythrin (PE)-conjugated antibodies. Samples were kept for 1 h at room temperature protected from light prior to injection into the AF4 channel. Plasma samples were diluted 1:1 in PBS, spiked with EVs separated from cell culture supernatant when specified and incubated with PE-conjugated antibodies. Urine samples were diluted 1:1 in PBS, spiked with LNCaP-derived EVs when specified, and incubated with PE-conjugated antibodies. For control experiments, plasma samples were diluted 1:1 in PBS, spiked with soluble EpCAM (cat no. SRP6455, Merck Life Science) or soluble HER2 (cat no. SRP6405, Merck Life Science) in different concentrations and incubated with PE-conjugated antibodies.

The following antibodies were used for AF4-MALS-FLD experiments: PE mouse monoclonal anti-CD9 (0.1 μg/test) (cat no. 12-0098-42, Thermo Fisher Scientific), PE mouse monoclonal anti-CD63 (0.1 μg/test) (cat no. 12-0639-42, Thermo Fisher Scientific), PE mouse monoclonal anti-CD81 (5 μL/test) (cat no. A15781, Thermo Fisher Scientific), PE mouse monoclonal anti-PSMA (0.1 μg/test) (cat no. 342503, Biolegend), PE mouse monoclonal anti-EpCAM (0.25 μg/test) (cat no. 566841, BD biosciences), PE mouse monoclonal anti-HER2 (0.1 μg/test) (cat no. 340552, BD biosciences) and PE mouse monoclonal isotype control (0.1 μg/test) (cat no. 550617, BD biosciences).

2.11 | Asymmetrical Flow Field-Flow Fractionation (AF4)

An AF4 long channel with a frit inlet coupled to the Eclipse system (Wyatt Technology) was driven by an isocratic pump system including a degasser and an autosampler (Shimadzu). Detection was performed by an ultraviolet (UV) detector at 280 nm (Shimadzu), a multi-angle light scattering (MALS) detector DAWN HELEOS-II using a laser at 658 nm (Wyatt Technology) and a fluorescence detector (FLD) with an excitation at 488 nm, emission at 578 nm and a gain of 16 (Agilent Technologies) (Geeurickx et al. 2021). The channel was set up with a 350 μm spacer and a 10 kDa regenerated cellulose (RC) membrane (165642-10, Wyatt Technology). PBS supplemented with 0.02% w/v NaN_3 (cat no. S0489, TCI Chemicals) and filtered with a 0.1 μm polyethersulfone (PES) filter (cat no. S2VPU02RE, Merck Life Science) was used as a mobile phase. All runs were performed at room temperature (20°C–25°C).

A detector flow of 0.5 mL/min was applied in the channel, and the sample was injected with an injection flow rate of 0.2 mL/min. An initial crossflow of 2.5 mL/min for 5 min was applied. Subsequently, the crossflow decreased linearly from 2.5 mL/min to 0.2 mL/min over 30 min. The crossflow was kept constant at 0.2 mL/min for 15 min after which a linear decrease in crossflow from 0.2 to 0.1 mL/min over 15 min was applied. The crossflow was again kept constant at 0.1 mL/min for 15 min. The protocol was finished by cleaning the channel from all remaining components using a crossflow of 0 mL/min for 20 min. The elution inject mode was used during the entire run.

The Voyager software (Wyatt Technology) was used for data acquisition, and the Astra software version 7.3.2 (Wyatt Technology) was used for data analysis. Baseline subtraction was performed. The area under the curve of the fluorescent signal was quantified for each run. When analysing pre-purified EVs from cell culture supernatant, the area under the curve starting from 24 min up to 80 min was calculated; when analysing complex matrix samples (cell culture supernatant, urine, or plasma), the time range between 40 min and 80 min was calculated. For size distribution analysis, the number density method was applied using the sphere model as previously described (Geeurickx et al. 2021). The refractive index for EVs (1.37) was added for correct number density estimation (Geeurickx et al. 2019).

2.12 | Liquid chromatography-tandem mass spectrometry (LC-MS/MS)

Samples were collected from the AF4-MALS-FLD run. Fractions 40–80 min were collected and concentrated using Amicon Ultra-2 and Amicon Ultra-15 centrifugal filters with a 10 kDa nominal molecular weight limit (cat no. UFC201024, Merck Life Science). Samples were processed for LC-MS/MS by filter-aided sample preparation (FASP) (Dhondt et al. 2020). Lysates were prepared by mixing samples with lysis buffer (2% SDS, 500 mM Tris-HCl (pH 7.6), 0.5 M dithiothreitol (DTT)) at a 4:1 sample-to-buffer ratio and incubated at 95°C for 5 min. Lysates were clarified by centrifugation at 16,000 g for 1 min. Lysates were mixed with 300 µL UA buffer (8 M urea, 0.1 M Tris-HCl (pH 8.5)) in a Microcon YM-10 centrifugal filter (cat no. MRCPRT010, Merck Life Science). Filters were centrifuged at 14,000 g for 40 min at 20°C until the filter unit was almost dry. 200 µL of UA buffer was added to the filter and centrifuged again at 14,000 g for 40 min. Proteins were alkylated by addition of 100 µL IAA solution (0.05 M iodoacetamide in UA buffer), mixed for 1 min at 37°C and incubated for 30 min at room temperature. The filters were centrifuged at 14,000 g for 30 min. This was followed by the addition of two times 100 µL UA buffer and two times 100 µL DB buffer (1 M urea, 0.1 M Tris-HCl (pH 8.5)) with a centrifugation of 14,000 g for 30 min in between. Filters were transferred to new collection tubes, and 40 µL of DB with Trypsin/Lys-C mix (cat no. V5073, Promega) was added in a 1:25 enzyme-to-protein ratio. After mixing for 1 min at 37°C samples were incubated overnight at 37°C for proteolytic digestion. Digests were collected by addition of 100 µL DB buffer and centrifugation for 15 min at 14,000 g. This step was repeated once.

Collected peptides were acidified with 0.5% trifluoroacetic acid to a pH of 2–3, followed by desalting with C18-StageTips (C18 Empore Disks, cat no. 051115-08808, 3 M). Desalted peptides were vacuum dried, dissolved in 0.1% formic acid and loaded on a nanoflow high-performance liquid chromatography (HPLC) system (Easy-nLC1000, Thermo Fisher Scientific) coupled to a Q Exactive HF Hybrid Quadrupole-Orbitrap Mass Spectrometer (Thermo Fisher Scientific) equipped with a nano-electrospray ionisation source. The mobile phase consisted of 0.1% formic acid (solvent A) and acetonitrile/water (95:5 (v/v)) with 0.1% formic acid (solvent B). The peptides were separated with a 40 min gradient from 8%–35% of solvent B. Before the end of the run, the percentage of solvent B was raised to 100% in 5 min and kept there for 5 min. A full MS scan over the mass-to-charge (m/z) range of 300–1750 with a resolution of 120,000, followed by data-dependent acquisition (DDA) with an isolation window of 2.0 m/z and a dynamic exclusion time of 20 s was performed. The top 12 ions were fragmented by higher energy collisional dissociation with a normalised collision energy of 27% and scanned over the m/z range of 200–2000 with a resolution of 15,000. After the MS2 scan for each of the top 12 ions had been obtained, a new full mass spectrum scan was acquired, and the process repeated until the end of the 50 min run.

Tandem mass spectra were searched using the MaxQuant software (version 1.6.10.43) against reviewed human sequences of UniProtKB release 2021_02. Peptide-spectrum-match and protein-level false discovery rates were set at 0.01. Carbamidomethyl (C), as a fixed modification, and oxidation (M) and acetylation of the protein N-terminus as dynamic modifications were included. A maximum of two missed cleavages by trypsin/LysC was allowed. The LC-MS profiles were aligned, and the identifications were transferred to non-sequenced or non-identified MS features in other LC-MS runs (matching between runs). The protein was determined as detected in the sample if its identification had been derived from at least two unique peptide identifications. Label-free quantification (LFQ) was performed using the MaxLFQ algorithm integrated into the MaxQuant software. The LFQ intensity was log2-transformed, and intensities were transformed to z-scores.

For targeted detection of PSMA (FOLH1), a parallel reaction monitoring (PRM) acquisition method using precursor m/z values of seven FOLH1 tryptic peptides with charge +2 and/or charge +3 was employed. The isolation window was 1.6 m/z with 0.3 m/z offset. The start and end retention times of the precursors were determined from previous DDA runs of the same samples. The results were analysed using Skyline (version 20.2.0.343). The sum of the best two or three b and y ion peak areas of the best three precursor ions was calculated, and the intensities were transformed to z-scores.

The mass spectrometry proteomics data have been deposited to the ProteomeXchange Consortium via the PRIDE partner repository (Perez-Riverol et al. 2022) with the dataset identifier PXD031264. The PRM data is available at PanoramaWeb (panoramaweb.org/31VlCW.url).

2.13 | Statistical Analysis

Data visualisation and statistical analyses were performed in GraphPad Prism version 8.4.3 (GraphPad Software). Differences in mean values between groups were analysed by the Mann-Whitney test. Correlation was analysed using linear regression. The limit of detection (LOD) was calculated by multiplying the standard deviation of the y-value by 3.3 and dividing by the slope of the regression curve (Anderson 1989). P-values smaller than 0.05 were considered statistically significant. For patient urine samples, the protein intensity levels and AF4-MALS-FLD peak area values were transformed to z-scores. For patient plasma samples, the AF4-MALS-FLD peak area was normalised for the mean signal of the control group.

2.14 | EV-TRACK

We have submitted all relevant data of our experiments to the EV-TRACK knowledgebase (EV-TRACK ID: EV210212) (EVtrack.org) (Van Deun et al. 2017).

3 | Results

3.1 | Set-up of the One-Step AF4-MALS-FLD Workflow for EV Size and Surface Marker Detection

To set up the AF4-MALS-FLD workflow, we used EVs prepared by ODG centrifugation from cell culture supernatant of selected prostate (LNCaP) and breast (MCF-7, MDA-MB-231 and SK-BR-3) cancer cell lines characterised by differential surface biomarker

presence (PSMA, EpCAM and HER2) (Table S4). EVs were extensively characterised using western blotting, TEM, SMLM and NTA (Figures S1 and S2, Table S5) according to the current state-of-the-art and implemented as a sample or as a matrix spike. Complementary characterisation confirmed the specificity of the EV preparations and revealed the presence of the selected surface biomarkers.

Compared to EM and AF4-MALS, NTA showed a shift toward larger EV sizes, likely due to its lower detection limit (~70 nm), which excludes smaller, highly abundant EV subtypes (Gardiner et al. 2013). Furthermore, NTA measures hydrodynamic diameter, analysed by the particle's movement in suspension and therefore influenced by surface-bound macromolecules and the surrounding electrical double layer. AF4-MALS assesses the root mean square radius (R_{rms}), reflecting the average squared distance from the particle's center, and EM captures geometric diameter by directly imaging EVs and measuring their physical dimensions from high-resolution images (Chernyshev et al. 2015).

Next, we incubated ODG pre-purified EVs with PE-conjugated antibodies in BSA-containing buffer and injected the sample in the AF4 channel (Figure 1A). Different parameters of the AF4-MALS-FLD protocol were evaluated and altered to reach an optimal separation of unbound (free) antibodies from antibody-bound (labelled) EVs, including channel height (optimal setting: 350 µm spacer), membrane (optimal setting: 10 kDa RC membrane), detector flow (optimal setting: 0.5 mL/min), crossflow profile (optimal setting: 2.5 mL/min for 5 min, 2.5–0.2 mL/min (linear) for 30 min, 0.2 mL/min for 15 min, 0.2–0.1 mL/min (linear) for 15 min, 0.1 mL/min for 15 min and 0 mL/min for 20 min), and fluorescence detector gain (optimal setting: 16) (Figure S3). The light scatter signal and UV signal (280 nm) are depicted in Figure 1B, with unbound antibodies eluting between 0 min and 24 min, and EVs starting to elute from 24 min. Size determination confirms the presence of EVs with an R_{rms} radius of 25–150 nm. The optimised AF4-MALS-FLD workflow was validated using PE-conjugated antibodies for EV surface marker proteins CD9, CD63 and CD81, confirming the presence of EVs in fractions eluting between 24 and 80 min (Figure 1C). TEM images further support the abundant presence of EVs in fraction 24–80 min, with 96% of EVs eluting in this fraction (Figure 1D). When the crossflow dropped to zero (at 80 min), all remaining sample components eluted from the channel.

3.2 | AF4-MALS-FLD Detection Confirms Size and Surface Biomarker Analysis of Purified EV Preparations

To optimise the labelling procedure for PSMA, EpCAM and HER2, EVs prepared by ODG centrifugation from cell culture supernatant were incubated with different amounts (0.1 µg, 0.25 µg, 0.5 µg for PSMA and EpCAM; and 0.05 µg, 0.1 µg, or 0.2 µg for HER2) of PE-conjugated antibodies, and the condition with the optimal signal-to-noise ratio was selected for further experiments (PSMA 0.1 µg, EpCAM 0.25 µg and HER2 0.1 µg) (Figure S4). Subsequently, EVs (4×10^{10} particles) prepared by ODG centrifugation from cell culture supernatant of three breast cancer cell lines (MCF-7, MDA-MB-231 and SK-BR-3) were labelled with PE-conjugated anti-EpCAM or anti-HER2 antibodies (0.25 µg and 0.1 µg for EpCAM and HER2, respectively) (Figure 2A-C). Size distributions in the 24–80 min fraction ranged from 29–120 nm, 28–183 nm and 30–166 nm in R_{rms} for MCF-7, MDA-MB-231 and SK-BR-3 EVs, respectively. The area under the curve of the fluorescence fractogram between 24 and 80 min was implemented as a measure for marker quantification (Figure 2D). MCF-7 and SK-BR-3 EVs were enriched in EpCAM, whereas only SK-BR-3 EVs were enriched in HER2, confirming western blot and SMLM results on breast cancer cells and their EV preparations (Figure S1).

Next, we analysed the fluorescence signal obtained for different numbers of prostate and breast cancer-derived EVs as measured by NTA. Different numbers of EVs separated from LNCaP cells (high PSMA expression), ranging from 6×10^9 to 2×10^{10} particles, including a negative control (no particles), were labelled with PE-conjugated anti-PSMA antibodies (Figure 2E). Quantification of the AF4-MALS-FLD peak area (24–80 min) revealed a linear correlation with the number of labelled particles as measured by NTA (R^2 of 0.9575) (Figure 2F). Subsequently, different numbers of EVs separated from MCF-7 cells (high EpCAM expression), ranging from 2×10^{10} to 6×10^{10} particles, including a negative control (no particles), were labelled with PE-conjugated anti-EpCAM antibodies (Figure 2G). Quantification of the AF4-MALS-FLD peak area (24–80 min) revealed a linear correlation with the number of labelled particles as measured by NTA (R^2 of 0.9225) (Figure 2H). Similarly, AF4-MALS-FLD detection of EVs separated from SK-BR-3 cells (high HER2 expression) labelled with PE-conjugated anti-HER2 antibodies showed a linear correlation in the range of 2×10^{10} to 6×10^{10} particles (R^2 of 0.9633) (Figure 2I,J). Care must be taken not to overload the AF4 channel. At higher EV concentrations a greater proportion of EVs appears in the final fraction (fraction after 80 min), corresponding to the point at which the crossflow reaches zero.

3.3 | AF4-MALS-FLD Detection for EV Size and Surface Biomarker Analysis in Biofluids of Increasing Matrix Complexity

To evaluate the specificity and robustness of the AF4-MALS-FLD workflow, labelling of EVs in complex matrices was assessed. Different volumes of concentrated cell culture supernatant from MCF-7 cells were labelled with PE-conjugated anti-EpCAM antibodies. A linear correlation between AF4-MALS-FLD peak area and sample loading volume (0, 20, 40 and 60 µL of concentrated cell culture supernatant) was observed (R^2 of 0.9491) (Figure 3A). Due to the presence of small non-EV particles eluting until 40 min and the absence of EVs eluting before 40 min, the area under the curve was obtained for EVs eluting from 40 to 80 min (Figures S5 and S6).

To further increase the complexity of the matrix, urine of a healthy volunteer (concentrated 10 times) was spiked with pre-purified prostate cancer cell-derived EVs in different clinically relevant concentrations (6×10^9, 8×10^9 and 10×10^9 particles, including a negative control (no particles)). Hereto, urine was diluted 1:1 with PBS to reduce the viscosity of the sample. AF4-MALS-FLD quantification detected EVs over the entire concentration range, revealing a linear correlation between FLD peak area and particle concentration as detected by NTA (R^2 of

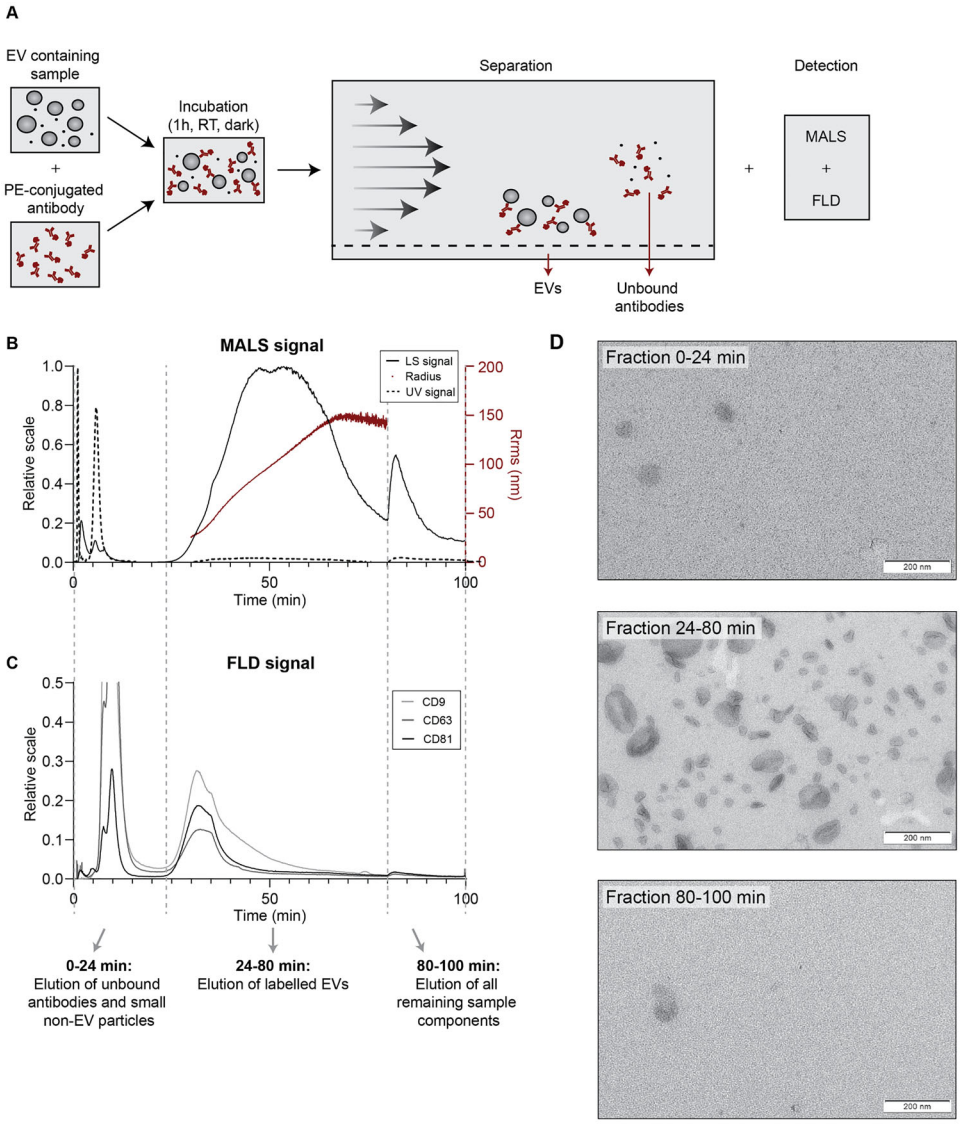

FIGURE 1 | Representation and validation of the AF4-MALS-FLD method. (A) Overview of the workflow used for identification of EV surface proteins. PE-conjugated antibodies were incubated with the sample (e.g. pre-purified EVs, cell culture supernatant, urine, or plasma) and loaded into the AF4 channel. (B) The light scatter elution profile (in relative scale) (black, full line), UV elution profile (black, dotted line) and the size determination (R_{rms} in nm) (red) obtained by the multi-angle light scattering (MALS) detector is plotted against time for labelling of SK-BR-3-derived EVs with PE-conjugated anti-CD81 antibody. (C) The fluorescent light detector (FLD) signal (in relative scale) for SK-BR-3-derived EVs labelled with PE-conjugated anti-CD9, anti-CD63 and anti-CD81 is plotted against time. (D) Transmission electron microscopy (TEM) images of different fractions of the AF4-MALS-FLD elution profile are shown (scale bar = 200 nm).

0.9921) (Figure 3B). The limit of detection (LOD) was 7.18×10^8 particles.

Lastly, we evaluated the potential of AF4-MALS-FLD to detect pre-purified EVs spiked in blood plasma. Blood plasma of a healthy volunteer (100 µL) was diluted 1:1 with PBS and spiked with increasing concentrations of MCF-7 or SK-BR-3 EVs and subsequently labelled with PE-conjugated anti-EpCAM or anti-HER2 antibodies, respectively. The concentration of EVs in blood plasma of breast cancer patients was previously described to range from 5×10^9 to 4×10^{10} particles/100 µL. A dose-dependent increase in FLD peak area was observed, and a linear correlation was achieved between 4×10^9 and 6×10^{10} EVs (R^2 of 0.9736 and 0.9861 for MCF-7 EpCAM labelling and SK-BR-3 HER2 labelling, respectively). EVs were detected over the entire concentration range, and LOD values of 2.13×10^9 and 1.53×10^9 particles for EpCAM and HER2 labelling were obtained, respectively (Figure 3C,D).

Labelling of different concentrations of SK-BR-3 EVs with isotype controls confirmed that non-specific signals in the control samples were negligible and revealed no alterations in FLD peak area upon increasing EV concentration (Figure 3D). Furthermore, soluble EpCAM or HER2 protein spiked in the blood plasma of a healthy volunteer in different clinically relevant concentrations (0, 1, 5 and 10 ng/mL for EpCAM and 0, 50, 100 and 150 ng/mL for HER2; Figure 3E) did not impact the AF4-MALS-FLD peak area estimation. These results demonstrated that

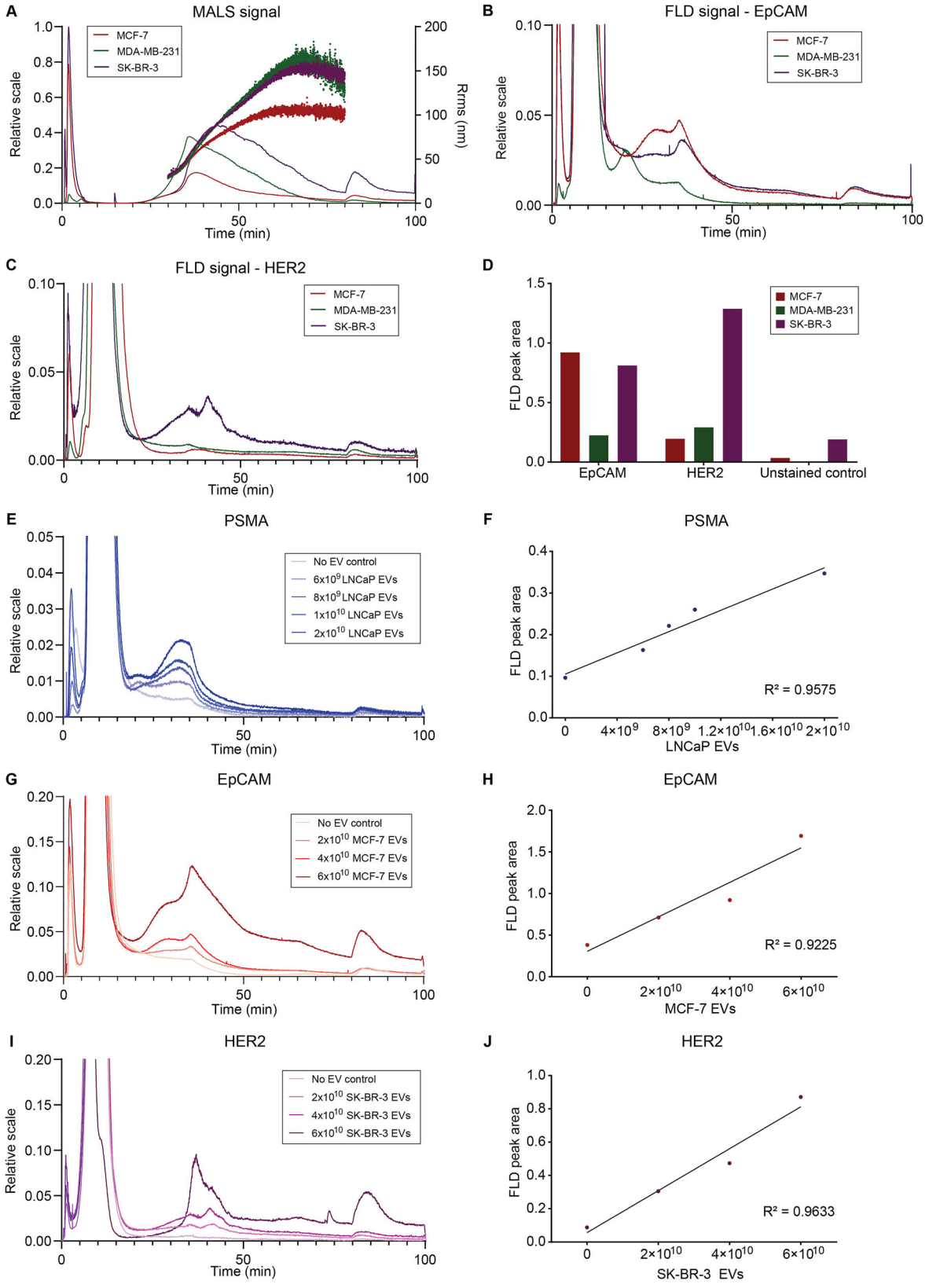

FIGURE 2 | Legend on next page.

AF4-MALS-FLD successfully detects spiked EVs in complex biofluids without a priori biofluid processing steps, further emphasising the specificity and robustness of the established protocol.

3.4 | Proof-of-Concept of AF4-MALS-FLD-Based EV Size and Surface Biomarker Analysis in Biofluids From Cancer Patients Versus Healthy Donors

Urine from five prostate cancer patients was collected, labelled for PSMA and processed through the AF4-MALS-FLD workflow to evaluate the ability of the workflow to detect size and EV-associated surface biomarkers of urinary EVs (Table S1). Proteomic analysis of the EV-containing fraction eluting between 40 and 80 min revealed the presence of EV-associated proteins Syntenin-1, Flotillin-1, CD63, CD9, Flotillin-2, Alix and TSG101 in all, and CD81 in four out of five urine samples (Figure 4A). Targeted proteomic analysis using precursor m/z values of seven FOLH1 tryptic peptides demonstrated detection of PSMA in all patient samples. PSMA analysis by AF4-MALS-FLD correlated with PSMA detection by proteomic analysis (Pearson's $r = 0.9372$, $p = 0.0187$) (Figure 4B).

Blood plasma from breast cancer patients versus sex-matched healthy donors was collected and labelled for HER2 or EpCAM to evaluate the differentiation capacity of the AF4-MALS-FLD workflow (Table S2 and S3). HER2 labelling directly in blood plasma distinguished HER2-amplified breast cancer patients ($n = 10$) from healthy controls ($n = 7$) ($p = 0.0036$) (Figure 4C). Similarly, EpCAM labelling differentiated breast cancer patients ($n = 8$) from healthy donors ($n = 6$) ($p = 0.0200$) (Figure 4D).

4 | Discussion

EVs have gained increasing interest in cancer research because of their high diagnostic and prognostic potential. Unlike tissue biopsies, liquid biopsies can be obtained non-invasively. Furthermore, while tissue biopsies reflect only a specific profile within a heterogeneous tumour, liquid biopsies can potentially overcome this limitation by providing a more comprehensive view of the entire tumour landscape, including metastases (Kalluri 2016). Although multiple EV-related biomarkers have been proposed, their clinical implementation is hindered by the lack of fast, simple and sensitive detection methods specifically quantifying EV-associated biomarkers (Geeurickx and Hendrix 2020).

We optimised an EV surface marker characterisation workflow in which AF4 was used to (a) separate labelled EVs from free antibody without the need for any additional pre-processing steps, (b) remove soluble ectodomains of transmembrane protein surface markers, which are known to hamper the detection of EV-associated biomarkers and (c) simplify the complex matrix. Biofluids contain high concentrations of non-EV particles such as Tamm-Horsfall protein (THP) polymers and albumin in urine, and immunoglobulins and lipoprotein particles in blood plasma. Size-based separation techniques, including AF4 allow us to separate EVs from part of the THP polymers in urine as well as ApoA1-positive and part of the ApoB-positive lipoproteins in blood plasma (Kim et al. 2020; Wu et al. 2020; Oeyen et al. 2018). Although size-based separation reduces the overall complexity of the biofluid, it does not completely eliminate non-EV components of similar size, such as very-low-density lipoproteins and chylomicrons. These residual particles can still interfere with downstream analyses, including metrics like size analysis.

Integrating a MALS detector downstream of the AF4 channel allows for highly accurate size and number density estimation of the particles, outperforming current methodology used in the EV research field (Vogel et al. 2021). This approach confirms the presence of particles between 30 and 1000 nm in the EV-rich fractions. The integration of a UV detector allows real-time tracking of molecules as they elute from the AF4 channel by measuring their absorbance at a specific wavelength. Monitoring at 280 nm is especially useful since antibodies strongly absorb at this wavelength, and although EVs are mainly composed of lipids, they still show absorbance at 280 nm because of proteins associated to the surface or encapsulated inside the EVs. Unexpected protein peaks in the EV-rich fraction may indicate insufficient separation of non-EV components and/or antibodies. The in-line inclusion of the FLD further allows direct detection of fluorophore-tagged antibodies targeting EV surface markers as well as potential cancer biomarkers. The AF4-MALS-FLD workflow therefore allows to separate EVs and analyse EV surface markers in a one-step process without the need for additional handling steps and therefore reducing operator-induced variability. Furthermore, the AF4-MALS-FLD workflow requires less than 3 h to perform separation and characterisation of EVs from urine and blood plasma samples and only 5 min hands-on time, while the turnaround time of current EV preparation protocols lies between 3 and 22 h, removal of unbound antibodies requires 0.5 h to 2.5 h and EV surface marker characterisation requires

FIGURE 2 | AF4-MALS-FLD analysis of EV surface proteins with biomarker potential in prostate and breast cancer. MCF-7-, MDA-MB-231- and SK-BR-3-derived EVs were labelled with PE-conjugated anti-EpCAM antibodies and analysed by AF4-MALS-FLD. (A) The elution profile (in relative scale) of the multi-angle light scatter (MALS) detector and the size (R_{rms} in nm) were plotted against time. The fluorescent light detector (FLD) signal for MCF-7-, MDA-MB-231- and SK-BR-3-derived EVs labelled with (B) PE-conjugated anti-EpCAM and (C) PE-conjugated anti-HER2 antibodies were plotted. (D) From FLD elution profiles, the area under the curve for the EV peak (24–80 min) was determined. Unstained EV samples were used as a negative control. (E) Different concentrations (6×10^9, 8×10^9, 1×10^{10} and 2×10^{10} particles as measured by NTA) including a negative control of LNCaP-derived EVs (high PSMA expression) were labelled with anti-PSMA antibodies and analysed by the AF4-MALS-FLD protocol. (F) The area under the curve for the EV peak was determined for LNCaP-derived EVs. Different concentrations (2×10^{10}, 4×10^{10} and 6×10^{10} particles as measured by NTA) including a negative control of (G) MCF-7-derived EVs (high EpCAM expression) or (I) SK-BR-3-derived EVs (high HER2 expression) were labelled with PE-conjugated anti-EpCAM or anti-HER2 antibodies respectively and analysed by the AF4-MALS-FLD protocol. The area under the curve for the EV peak (24–80 min) was determined for (H) MCF-7- and (J) SK-BR-3-derived EVs.

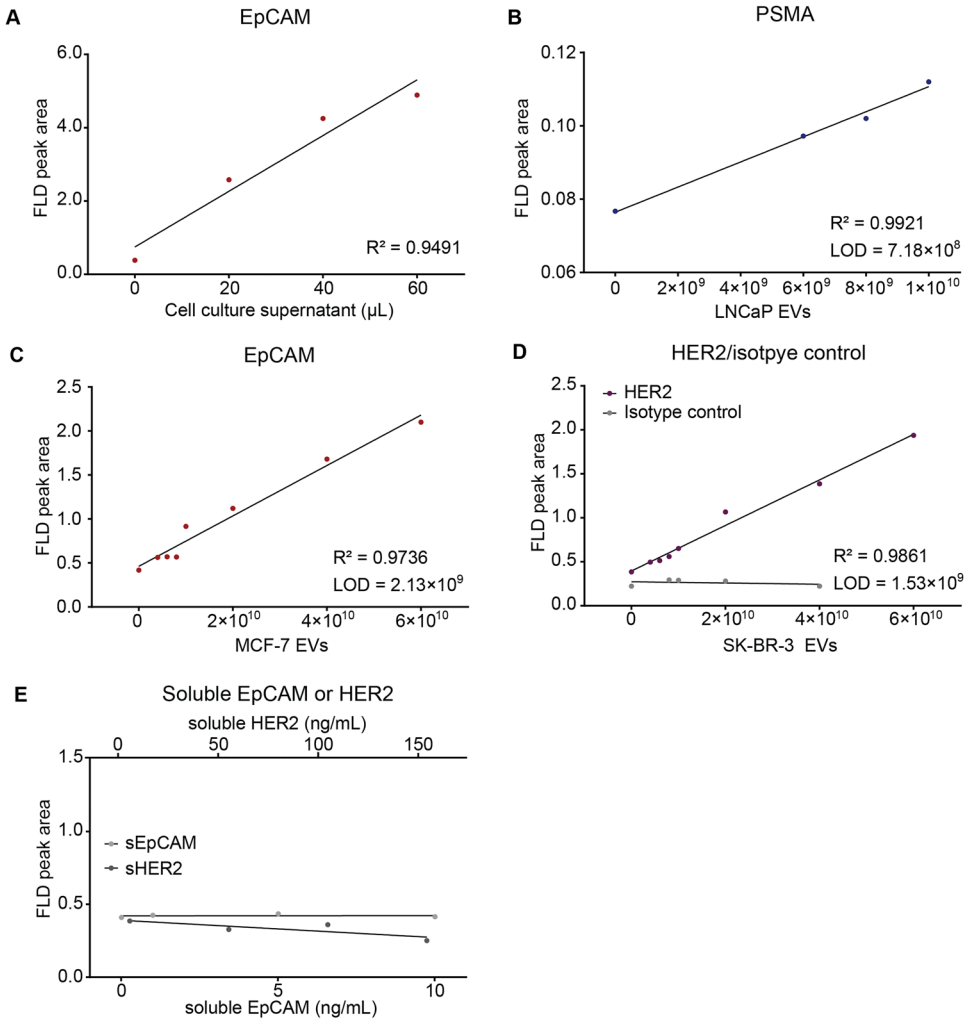

FIGURE 3 | **Detection of EVs in complex matrices**. (A) Different volumes of cell culture supernatant (0, 20, 40 and 60 µL) collected from the MCF-7 cells were labelled with PE-conjugated anti-EpCAM antibodies and analysed by AF4-MALS-FLD. The area under the curve for the EV peak in complex matrices (40–80 min) was determined. (B) Different amounts of LNCaP-derived EVs were spiked in 100 µL of concentrated urine, diluted 1:1 in PBS to reduce viscosity, labelled with PE-conjugated anti-PSMA antibodies, and analysed by AF4-MALS-FLD. The area under the curve for the EV peak was determined. Different amounts of (C) MCF-7- or (D) SK-BR-3-derived EVs were spiked in 100 µL of blood plasma, diluted 1:1 in PBS to reduce viscosity, and labelled with PE-conjugated anti-EpCAM or anti-HER2 antibodies, respectively. Labelled EVs were analysed by AF4-MALS-FLD and the area under the curve for the EV peak was determined. Different amounts of SK-BR-3 EVs were also spiked in blood plasma and labelled with isotype control antibodies. (E) Different concentrations of soluble EpCAM (1, 5 and 10 ng/mL) and soluble HER2 (50, 100 and 150 ng/mL) were spiked in blood plasma, labelled with PE-conjugated anti-EpCAM or anti-HER2 antibodies respectively, and analysed by AF4-MALS-FLD.

multiple hours (Hendrix et al. 2023). In contrast to current EV methodology, also only small volumes (100 µL) of biofluids are needed for AF4-MALS-FLD analysis.

The AF4-MALS-FLD workflow demonstrated the detection of EV surface markers in samples with increasing complexity, starting from EV samples separated by density gradient centrifugation and characterised using state-of-the-art technology as presented by the MISEV guidelines (Van Deun et al. 2017; Théry et al. 2018), to cell culture supernatant and even urine and blood plasma samples spiked with clinically relevant concentrations of EVs (Dhondt et al. 2020; Vergauwen et al. 2021). Furthermore, analysis of patient samples proved the AF4-MALS-FLD workflow effective in detecting EVs positive for cancer biomarkers such as PSMA, EpCAM and HER2.

The AF4-MALS-FLD workflow was compared to existing EV surface marker detection methods (Table 1). Most techniques require prior EV separation from the biofluid, such as urine and blood plasma. Detection of EV markers directly in the biofluid is not frequently performed, as the presence of high-abundant proteins and the soluble form of the marker influence the results. In contrast, AF4-MALS-FLD analysis integrates in situ EV size-based separation with EV surface marker characterisation, eliminating the need for pre-purification. Furthermore, many other techniques need removal of unbound antibodies by including washing steps, while this is not necessary for the AF4-MALS-FLD workflow. Additionally, EV-rich fractions collected during AF4-MALS-FLD analysis can be retrieved for further characterisation, while this is less straightforward for many capture-based techniques. Similar to our approach, a liquid

TABLE 1 | Comparison of EV surface marker characterisation methods in relation to fundamental evaluation performances.

	Pre-purification necessary	In situ EV separation	Size characterisation	Quantitative surface marker analysis	Washing steps after antibody labelling necessary	Sensitivity	Further downstream analysis possible	References
AF4-MALS-FLD	No	Yes	Yes	Yes	No	High	Yes	Lippens et al.
Western blot	Yes	No	No	Yes	Yes	Low	No	(BöIng et al. 2014, Kowal et al. 2017)
ELISA	Yes/No	No	No	Yes	Yes	Low	No	(Logozzi et al. 2009)
Bead-based FCM	Yes	Yes	No	Yes	Yes	Interm.	No	(Suárez et al. 2017)
immuno-EM	Yes	No	Yes	No	No	Low	No	(Brisson et al. 2017)
Fluorescent NTA	Yes	No	Yes	Yes	Yes	Interm.	Yes	(Thane et al. 2019)
High resolution FCM	Yes	Yes	Yes	Yes	No	High	Yes	(Tian et al. 2018, van der Vlist et al. 2012)
SP-IRIS	No	No	Yes	Yes	Yes	High	No	(Daaboul et al. 2016)
TAS	No	No	No	Yes	No	High	No	(Tian et al. 2021)
LFIA	Yes	No	No	Yes	No	Interm.	No	(Moyano et al. 2021, Oliveira-Rodríguez et al. 2016)
SPR	No	No	No	Yes	Yes	High	No	(Yildizhan et al. 2021, Grasso et al. 2015, Rupert et al. 2014, Im et al. 2014)
Au-NPFe2O3NC	No	No	No	Yes	Yes	High	No	(Yamauchi et al. 2019)
µNMR	Yes	Yes	No	Yes	Yes	High	Yes	(Shao et al. 2012)
iMEX	No	No	No	Yes	Yes	High	No	(Jeong et al. 2016)
ExoScreen	No	No	No	Yes	No	High	No	(Yoshioka et al. 2014)
SEA	Yes	No	No	Yes	Yes	High	No	(Lee et al. 2018)

Colour indication: green = preferential status; orange = non-preferential status; light orange = intermediate.

AF4-MALS-FLD, asymmetrical flow field-flow fractionation - multi-angle light scattering - fluorescent light detection; ELISA, enzyme-linked immunosorbent assay; FCM, flow cytometry; EM, electron microscopy; NTA, nanoparticle tracking analysis, SP-IRIS, single-particle-interferometric reflectance imaging sensor; TAS, thermophoretic aptasensor; LFIA, lateral flow immunoassay; SPR, surface plasmon resonance; Au-NPFe_2O_3NC, gold-loaded ferric oxide nanocubes; µNMR, micro-nuclear magnetic resonance; iMEX, integrated magnetic-electrochemical exosome; SEA, single EV analysis.

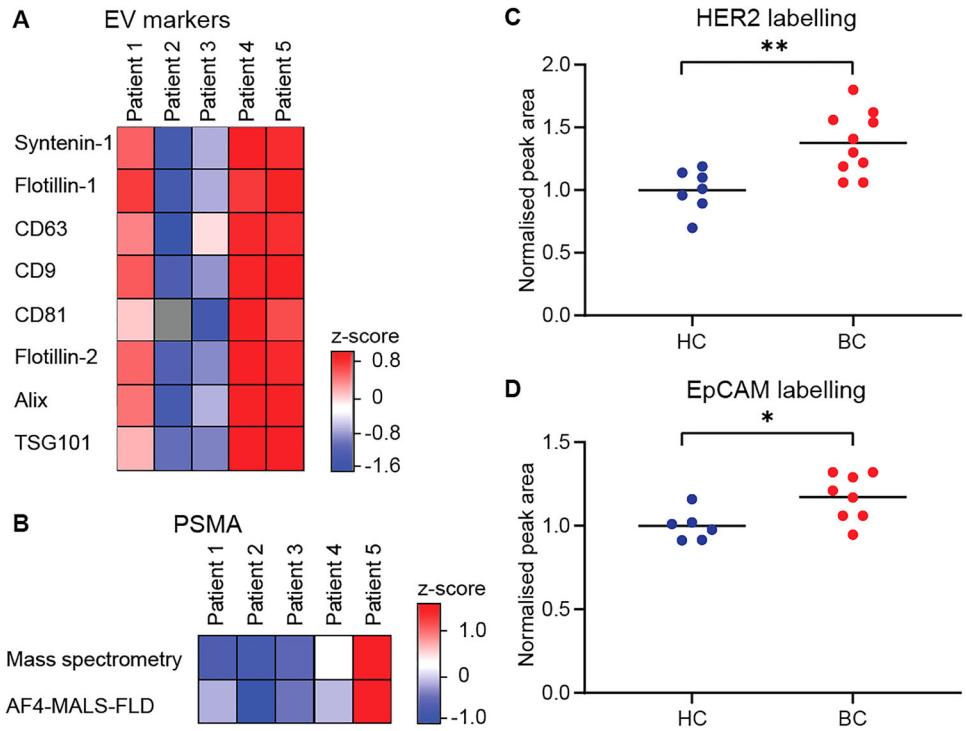

FIGURE 4 | **Validation of the AF4-MALS-FLD workflow on patient samples**. Urine samples of five prostate cancer patients were labelled for PSMA and analysed by the AF4-MALS-FLD workflow. Fractions 40–80 min were collected, concentrated and processed for mass spectrometry-based proteomic analysis. (A) EV markers Syntenin-1, Flotillin-1, CD63, CD9, CD81, Flotillin-2, Alix and TSG101 were analysed (missing sample indicated in grey). *Z*-score transformation of intensities were plotted. (B) Targeted mass spectrometry analysed the presence of PSMA (FOLH1) in patient samples. The *z*-score transformation of intensities was plotted with the AF4-MALS-FLD peak area. (C) Blood plasma samples of healthy controls ($n = 7$) and HER2 amplified breast cancer patients ($n = 10$) were labelled with PE-conjugated anti-HER2 antibodies. (D) Blood plasma samples of healthy controls ($n = 6$) and breast cancer patients ($n = 8$) were labelled with PE-conjugated anti-EpCAM antibodies. The area under the curve values were normalised for the mean value in the healthy control group.

chromatography(LC)-MALS-FLD workflow has been optimised for surface marker labelling, lumen labelling and lipid membrane labelling of EVs (Normak et al. 2023). However, separation by AF4 has multiple advantages over other size-based separation methods such as LC. AF4 is less prone to clogging and is more flexible in protocol optimisation increasing separation efficiency. Furthermore, AF4 results in reduced shear forces applied to the EVs and EVs are less prone to clumping and deformation (Linares et al. 2015).

The study has a few limitations. First, multiplexed detection of EV surface markers was not performed. However, this would allow us to decrease analysis time and reduce sample volume when analysing multiple biomarkers. Second, due to the proof-of-concept nature of this technical note, the method's technical repeatability and reproducibility, as well as detection sensitivity and specificity were not evaluated. Nonetheless, future studies should rigorously incorporate repeated measurements for each surface marker to ensure methodological reliability. Third, while we established proof-of-concept using clinical samples, validation in a larger patient cohort is still needed. Fourth, by considering the 40–80 min elution range for complex matrices, smaller EVs in the 30–50 nm size range (based on R_{rms} values from AF4-MALS) may be lost; however, TEM suggests that particles eluting before 40 min predominantly consist of non-vesicular material. Finally, although the AF4-MALS-FLD workflow is not restricted to the EV surface markers examined in this study, expanding it to a broader EV surface protein library may require optimisation of antibody concentration and incubation conditions for each surface marker as well as the most optimal EV concentration range. Furthermore, for each EV surface biomarker, a comparison of the AF4-MALS-FLD workflow with other surface marker-based detection methods should be performed to select the most suitable detection method for a certain application.

In conclusion, we established a one-step AF4-MALS-FLD workflow for the sensitive and rapid quantification of EV size and surface biomarkers in minute volumes of cell culture supernatant, urine, or blood plasma. AF4 enables separation of labelled EVs from unbound antibodies and smaller non-EV particles simultaneously with the characterisation of EV size and EV-associated surface biomarkers, resulting in reduced technical variability, analysis time, hands-on time and sample volume. To prove clinical utility, we demonstrated that this workflow detects EVs in urine from prostate cancer patients and discriminates blood plasma from breast cancer patients and healthy volunteers.

Author Contributions

Lien Lippens: conceptualisation, data curation, formal analysis, investigation, methodology, writing – original draft. **Niké Guilbert**: formal analysis, investigation, writing – original draft. **Sofie van Dorpe**: resources, data curation. **Sarah Deville**: funding acquisition, writing

– review and editing. **Robin Boiy**: investigation, methodology, formal analysis, data curation. **Quentin Roux**: investigation, methodology, formal analysis, data curation. **Nicolaas Lumen**: resources, data curation. **Ilkka Miinalainen**: investigation, methodology, formal analysis, data curation. **Pekka Rappu**: investigation, methodology, formal analysis, data curation, writing – review and editing. **Katrien Vandecasteele**: resources, data curation, writing – review and editing. **Hannelore Denys**: resources, data curation, writing – review and editing. **Bruno de Geest**: conceptualisation. **Olivier de Wever**: conceptualisation, supervision, writing – review and editing. **An Hendrix**: conceptualisation, supervision, funding acquisition, writing – review and editing. All authors reviewed the manuscript.

Acknowledgements

We thank Sofie De Geyter (Laboratory of Experimental Cancer Research, Department of Human Structure and Repair, Ghent University, Ghent, Belgium) for experimental support and Milena Hoorne (Medical Oncology, Department of Internal Medicine and Pediatrics, Ghent University Hospital, Ghent, Belgium) for sample collection. We also thank all members of the Laboratory of Experimental Cancer Research for discussion and support. We thank the proteomics and electron microscopy core facilities at the University of Turku and the University of Oulu, respectively, both supported by Biocenter Finland. Lastly, we thank the company Wyatt for the helpful discussions and support.

Funding

This work was supported by the Research Foundation Flanders (FWO) for funding received under PhD fellowships, a Postdoc fellowship and project funding (NG [11B9723N], SVD [11B3621N], LL [12D8123N] and AH [G023521N]), the European Research Council (ERC) for funding received under the European Union's Horizon 2020 research and innovation program (AH [101045156]), European Union's Horizon 2020 research and innovation program under the Marie Skłodowska-Curie (QR [722148]), Ghent University (SD, AH and ODW), the cancer research institute Ghent (CRIG) for funding received under a young investigator proof-of-concept project grant (LL and SD), and Kom op tegen Kanker (Stand up to Cancer), the Flemish cancer society (LL, AH and ODW).

Conflicts of Interest

The authors declare that they have no competing interests.

Ethics Approval

Urine samples were collected according to the approval of the ethical committee (EC/2019/1506) of Ghent University and in accordance with relevant guidelines. Collection of blood plasma samples was performed according to the approval of the ethical committee (EC/2014/0655) of Ghent University and in accordance with relevant guidelines.

Consent to Participate

Informed consent was obtained from all the study participants.

Data Availability Statement

The data that support the findings of this study are available from the corresponding author upon reasonable request.

References

Anderson, D. J. 1989. "Determination of the Lower Limit of Detection." *Clinical Chemistry* 35: 2152–2153. https://doi.org/10.1093/clinchem/35.10.2152.

Ashby, J., K. Flack, L. A. Jimenez, et al. 2014. "Distribution Profiling of Circulating MicroRNAs in Serum." *Analytical Chemistry* 86: 9343–9349. https://doi.org/10.1021/ac5028929.

BöIng, A. N., E. van der Pol, A. E. Grootemaat, et al. 2014. "Single-Step Isolation of Extracellular Vesicles by Size-Exclusion Chromatography." *Journal of Extracellular Vesicles* 3: 23430. https://doi.org/10.3402/jev.v3.23430.

Brisson, A. R., S. Tan, R. Linares, C. Gounou, and N. Arraud. 2017. "Extracellular Vesicles From Activated Platelets: A Semiquantitative Cryo-Electron Microscopy and Immuno-Gold Labeling Study." *Platelets* 28: 263–271. https://doi.org/10.1080/09537104.2016.1268255.

Chernyshev, V. S., R. Rachamadugu, Y. H. Tseng, et al. 2015. "Size and Shape Characterization of Hydrated and Desiccated Exosomes." *Anal Bioanal Chem* 407: 3285–3301. https://doi.org/10.1007/s00216-015-8535-3.

Costa-Silva, B., N. M. Aiello, A. J. Ocean, et al. 2015. "Pancreatic Cancer Exosomes Initiate Pre-Metastatic Niche Formation in the Liver." *Nature Cell Biology* 17: 816–826. https://doi.org/10.1038/ncb3169.

Daaboul, G. G., P. Gagni, L. Benussi, et al. 2016. "Digital Detection of Exosomes by Interferometric Imaging." *Scientific Reports* 6: 1–10. https://doi.org/10.1038/srep37246.

De Wever, O., and A. Hendrix. 2019. "A Supporting Ecosystem to Mature Extracellular Vesicles Into Clinical Application." *The EMBO Journal* 38, no. 9: e101412. https://doi.org/10.15252/embj.2018101412.

Dhondt, B., E. Geeurickx, J. Tulkens, et al. 2020. "Unravelling the Proteomic Landscape of Extracellular Vesicles in Prostate Cancer by Density-Based Fractionation of Urine." *Journal of Extracellular Vesicles* 9: 1736935. https://doi.org/10.1080/20013078.2020.1736935.

Dhondt, B., C. Pinheiro, E. Geeurickx, et al. 2023. "Benchmarking Blood Collection Tubes and Processing Intervals for Extracellular Vesicle Performance Metrics." *Journal of Extracellular Vesicles* 12: e12315. https://doi.org/10.1002/jev2.12315.

Fais, S., L. O'Driscoll, and F. E. Borras, et al. 2016. "Evidence-Based Clinical Use of Nanoscale Extracellular Vesicles in Nanomedicine." *ACS Nano* 10: 3886–3899. https://doi.org/10.1021/acsnano.5b08015.

Gardiner, C., Y. J. Ferreira, R. A. Dragovic, C. W. G. Redman, and I. L. Sargent. 2013. "Extracellular Vesicle Sizing and Enumeration by Nanoparticle Tracking Analysis." *Journal of Extracellular Vesicles* 2: 19671. https://doi.org/10.3402/jev.v2i0.19671.

Geeurickx, E., and A. Hendrix. 2020. "Targets, Pitfalls and Reference Materials for Liquid Biopsy Tests in Cancer Diagnostics." *Molecular Aspects of Medicine* 72: 100828. https://doi.org/10.1016/j.mam.2019.10.005.

Geeurickx, E., L. Lippens, P. Rappu, B. de Geest, O. De Wever, and A. Hendrix. 2021. "Recombinant Extracellular Vesicles as Biological Reference Material for Method Development, Data Normalization and Assessment of (pre-) Analytical Variables." *Nature Protocols* 16: 603–633. https://doi.org/10.1038/s41596-020-00446-5.

Geeurickx, E., J. Tulkens, B. Dhondt, et al. 2019. "The Generation and Use of Recombinant Extracellular Vesicles as Biological Reference Material." *Nature Communications* 10: 3288. https://doi.org/10.1038/s41467-019-11182-0.

Giddings, J. C., F. J. Yang, and M. N. Myers. 1976. "Flow Field-flow Fractionation: A Versatile New Separation Method." *Science* 193: 1244–1245. https://doi.org/10.1126/science.959835.

Grasso, L., R. Wyss, L. Weidenauer, et al. 2015. "Molecular Screening of Cancer-Derived Exosomes by Surface Plasmon Resonance Spectroscopy." *Analytical and Bioanalytical Chemistry* 407: 5425–5432. https://doi.org/10.1007/s00216-015-8711-5.

Hendrix, A. 2021. "The Nature of Blood(y) Extracellular Vesicles." *Nature Reviews Molecular Cell Biology* 22: 243. https://doi.org/10.1007/s00391-018-1445-1.

Hendrix, A., L. Lippens, C. Pinheiro, et al. 2023. "Extracellular Vesicle Analysis." *Nature Reviews Methods Primers* 3: 56. https://doi.org/10.1038/s43586-023-00240-z.

Hoshino, A., B. Costa-Silva, T.-L. Shen, et al. 2015. "Tumour Exosome Integrins Determine Organotropic Metastasis." *Nature* 527: 329–335. https://doi.org/10.1038/nature15756.

Im, H., H. Shao, Y. I. Park, et al. 2014. "Label-Free Detection and Molecular Profiling of Exosomes With a Nano-Plasmonic Sensor." *Nature Biotechnology* 32: 490–495. https://doi.org/10.1038/nbt.2886.Label-free.

Jeong, S., J. Park, D. Pathania, C. M. Castro, R. Weissleder, and H. Lee. 2016. "Integrated Magneto-Electrochemical Sensor for Exosome Analysis." *ACS Nano* 10: 1802–1809. https://doi.org/10.1021/acsnano.5b07584.

Kabe, Y., M. Suematsu, S. Sakamoto, et al. 2018. "Development of a Highly Sensitive Device for Counting the Number of Disease-Specific Exosomes in Human Sera." *Clinical Chemistry* 64: 1463–1473. https://doi.org/10.1373/clinchem.2018.291963.

Kalluri, R. 2016. "The Biology and Function of Exosomes in Cancer." *Journal of Clinical Investigation* 126: 1208–1215. https://doi.org/10.1038/nrc.2016.73.

Kamerkar, S., V. S. Lebleu, H. Sugimoto, et al. 2017. "Exosomes Facilitate Therapeutic Targeting of Oncogenic KRAS in Pancreatic Cancer." *Nature* 546: 498–503. https://doi.org/10.1038/nature22341.

Kim, Y. B., L. G. Bin, and M. H. Moon. 2022. "Size Separation of Exosomes and Microvesicles Using Flow Field-Flow Fractionation/Multiangle Light Scattering and Lipidomic Comparison." *Analytical Chemistry* 94: 8958–8965. https://doi.org/10.1021/acs.analchem.2c00806.

Kim, Y. B., J. S. Yang, L. G. Bin, and M. H. Moon. 2020. "Evaluation of Exosome Separation From human Serum by Frit-Inlet Asymmetrical Flow Field-Flow Fractionation and Multiangle Light Scattering." *Analytica Chimica Acta* 1124: 137–145. https://doi.org/10.1016/j.aca.2020.05.031.

Kowal, E. J. K., D. Ter-Ovanesyan, A. Regev, and G. M. Church. 2017. "Extracellular Vesicle Isolation and Analysis by Western Blotting." *Methods in Molecular Biology* 1660: 153–173. https://doi.org/10.1007/978-1-4939-7253-1_12.

Lee, K., K. Fraser, B. Ghaddar, et al. 2018. "Multiplexed Profiling of Single Extracellular Vesicles." *ACS Nano* 12: 494–503. https://doi.org/10.1021/acsnano.7b07060.

Linares, R., S. Tan, C. Gounou, N. Arraud, and A. R. Brisson. 2015. "High-Speed Centrifugation Induces Aggregation of Extracellular Vesicles." *Journal of Extracellular Vesicles* 4: 29509. https://doi.org/10.3402/jev.v4.29509.

Logozzi, M., A. de Milito, L. Lugini, et al. 2009. "High Levels of Exosomes Expressing CD63 and Caveolin-1 in Plasma of Melanoma Patients." *PLoS ONE* 4: e5219. https://doi.org/10.1371/journal.pone.0005219.

Menck, K., A. Bleckmann, A. Wachter, et al. 2017. "Characterisation of Tumour-Derived Microvesicles in Cancer Patients' blood and Correlation With Clinical Outcome." *Journal of Extracellular Vesicles* 6: 1340745. https://doi.org/10.1080/20013078.2017.1340745.

Moyano, A., E. Serrano-Pertierra, J. M. Duque, et al. 2021. "Magnetic Lateral Flow Immunoassay for Small Extracellular Vesicles Quantification: Application to Colorectal Cancer Biomarker Detection." *Sensors* 21: 3756. https://doi.org/10.3390/s21113756.

Normak, K., M. Papp, M. Ullmann, et al. 2023. "Multiparametric Orthogonal Characterization of Extracellular Vesicles by Liquid Chromatography Combined With in-Line Light Scattering and Fluorescence Detection." *Analytical Chemistry* 95: 12443–12451. https://doi.org/10.1021/acs.analchem.3c02108.

Oeyen, E., K. van Mol, G. Baggerman, et al. 2018. "Ultrafiltration and Size Exclusion Chromatography Combined With Asymmetrical-Flow Field-Flow Fractionation for the Isolation and Characterization of Extracellular Vesicles From Urine." *Journal of Extracellular Vesicles* 7: 1490143. https://doi.org/10.1080/20013078.2018.1490143.

Oliveira-Rodríguez, M., S. López-Cobo, H. T. Reyburn, et al. 2016. "Development of a Rapid Lateral Flow Immunoassay Test for Detection of Exosomes Previously Enriched From Cell Culture Medium and Body Fluids." *Journal of Extracellular Vesicles* 5: 31803. https://doi.org/10.3402/jev.v5.31803.

Perez-Riverol, Y., J. Bai, C. Bandla, et al. 2022. "The PRIDE Database Resources in 2022: A Hub for Mass Spectrometry-Based Proteomics Evidences." *Nucleic Acids Research* 50: D543–D552. https://doi.org/10.1093/nar/gkab1038.

Rupert, D. L. M., C. Lässer, M. Eldh, et al. 2014. "Determination of Exosome Concentration in Solution Using Surface Plasmon Resonance Spectroscopy." *Analytical Chemistry* 86: 5929–5936. https://doi.org/10.1021/ac500931f.

Shao, H., J. Chung, L. Balaj, et al. 2012. "Protein Typing of Circulating Microvesicles Allows Real-Time Monitoring of Glioblastoma Therapy." *Nature Medicine* 18: 1835–1841. https://doi.org/10.1038/nm.2994.

Suárez, H., A. Gámez-Valero, R. Reyes, et al. 2017. "A Bead-Assisted Flow Cytometry Method for the Semi-Quantitative Analysis of Extracellular Vesicles." *Scientific Reports* 7: 1–11. https://doi.org/10.1038/s41598-017-11249-2.

Thane, K. E., A. M. Davis, and A. M. Hoffman. 2019. "Improved Methods for Fluorescent Labeling and Detection of Single Extracellular Vesicles Using Nanoparticle Tracking Analysis." *Scientific Reports* 9: 1–13. https://doi.org/10.1038/s41598-019-48181-6.

Théry, C., K. W. Witwer, E. Aikawa, et al. 2018. "Minimal Information for Studies of Extracellular Vesicles 2018 (MISEV2018): A Position Statement of the International Society for Extracellular Vesicles and Update of the MISEV2014 Guidelines." *Journal of Extracellular Vesicles* 7: 1535750. https://doi.org/10.1080/20013078.2018.1535750.

Tian, F., S. Zhang, C. Liu, et al. 2021. "Protein Analysis of Extracellular Vesicles to Monitor and Predict Therapeutic Response in Metastatic Breast Cancer." *Nature Communications* 12: 1–13. https://doi.org/10.1038/s41467-021-22913-7.

Tian, Y., L. Ma, M. Gong, et al. 2018. "Protein Profiling and Sizing of Extracellular Vesicles From Colorectal Cancer Patients via Flow Cytometry." *ACS Nano* 12: 671–680. https://doi.org/10.1021/acsnano.7b07782.

Tkach, M., and C. Théry. 2016. "Communication by Extracellular Vesicles: Where We Are and Where to Go." *Cell* 164: 1226–1232. https://doi.org/10.1016/j.cell.2016.01.043.

van der Vlist, E. J., E. N. M. Nolte-'t Hoen, W. Stoorvogel, G. J. A. Arkesteijn, and M. H. M. Wauben. 2012. "Fluorescent Labeling of Nano-Sized Vesicles Released by Cells and Subsequent Quantitative and Qualitative Analysis by High-Resolution Flow Cytometry." *Nature Protocols* 7: 1311–1326. https://doi.org/10.1038/nprot.2012.065.

Van Deun, J., P. Mestdagh, P. Agostinis, et al. 2017. "EV-TRACK: Transparent Reporting and Centralizing Knowledge in Extracellular Vesicle Research." *Nature Methods* 14: 228–232. https://doi.org/10.1038/nmeth.4185.

Van Deun, J., P. Mestdagh, R. Sormunen, et al. 2014. "The Impact of Disparate Isolation Methods for Extracellular Vesicles on Downstream RNA Profiling." *Journal of Extracellular Vesicles* 3: 24858. https://doi.org/10.3402/jev.v3.24858.

Van Dorpe, S., L. Lippens, R. Boiy, et al. 2023. "Integrating Automated Liquid Handling in the Separation Workflow of Extracellular Vesicles Enhances Specificity and Reproducibility." *Journal of Nanobiotechnology* 21: 157. https://doi.org/10.1186/s12951-023-01917-z.

Van Dorpe, S., P. Tummers, H. Denys, and A. Hendrix. 2024. "Towards the Clinical Implementation of Extracellular Vesicle-Based Biomarker Assays for Cancer." *Clinical Chemistry* 70: 165–178. https://doi.org/10.1093/clinchem/hvad189.

Vergauwen, G., J. Tulkens, C. Pinheiro, et al. 2021. "Robust Sequential Biophysical Fractionation of Blood Plasma to Study Variations in the Biomolecular Landscape of Systemically Circulating Extracellular Vesicles Across Clinical Conditions." *Journal of Extracellular Vesicles* 10: e12122. https://doi.org/10.1002/jev2.12122.

Vogel, R., J. Savage, J. Muzard, et al. 2021. "Measuring Particle Concentration of Multimodal Synthetic Reference Materials and Extracellular Vesicles With Orthogonal Techniques: Who Is up to the Challenge?." *Journal of Extracellular Vesicles* 10: e12052. https://doi.org/10.1002/jev2.12052.

Wahlund, K. G., and J. C. Giddings. 1987. "Properties of an Asymmetrical Flow Field-Flow Fractionation Channel Having One Permeable Wall." *Analytical Chemistry* 59: 1332–1339. https://doi.org/10.1021/ac00136a016.

Wu, B., X. Chen, J. Wang, X. Qing, and Z. Wang. 2020. "Separation and Characterization of Extracellular Vesicles From human Plasma by Asymmetrical Flow Field- Flow Fractionation." *Analytica Chimica Acta* 1127: 234–245. https://doi.org/10.1016/j.aca.2020.06.071.

Yamauchi, Y., S. A. Hossain, N. Nguyen, and C. Salomon. 2019. "Avoiding Pre-Isolation Step in Exosome Analysis: Direct Isolation and Sensitive Detection of Exosomes Using Gold-Loaded Nanoporous Ferric Oxide Nanozymes." *Analytical Chemistry* 91: 3827–3834. https://doi.org/10.1021/acs.analchem.8b03619.

Yildizhan, Y., V. S. Vajrala, E. Geeurickx, et al. 2021. "FO-SPR Biosensor Calibrated With Recombinant Extracellular Vesicles Enables Specific and Sensitive Detection Directly in Complex Matrices." *Journal of Extracellular Vesicles* 10: e12059. https://doi.org/10.1002/jev2.12059.

Yoshioka, Y., N. Kosaka, Y. Konishi, et al. 2014. "Ultra-Sensitive Liquid Biopsy of Circulating Extracellular Vesicles Using ExoScreen." *Nature Communications* 5: 3591. https://doi.org/10.1038/ncomms4591.

Zhang, H., D. Freitas, H. S. Kim, et al. 2018. "Identification of Distinct Nanoparticles and Subsets of Extracellular Vesicles by Asymmetric Flow Field-Flow Fractionation." *Nature Cell Biology* 20: 332–343. https://doi.org/10.1038/s41556-018-0040-4.

Supporting Information

Additional supporting information can be found online in the Supporting Information section.

Supplementary Figure S1-S6 and Supplementary Table S1-S5